Aqueous harvesting of ^{88}Zr at a radioactive-ion-beam facility for cross-section measurements

Jennifer A. Shusterman,[1,2,*] Nicholas D. Scielzo,[3] E. Paige Abel,[4,5] Hannah K. Clause,[4,5] Nicolas D. Dronchi,[4] Wesley D. Frey,[6] Narek Gharibyan,[3] Jason A. Hart,[4] C. Shaun Loveless,[7] Sean R. McGuinness,[8] Logan T. Sutherlin,[9] Keenan J. Thomas,[3] Suzanne E. Lapi,[7] J. David Robertson,[9] Mark A. Stoyer,[3] Eric B. Norman,[10] Graham F. Peaslee,[8] Gregory W. Severin,[4,5] and Dawn A. Shaughnessy[3]

[1]*Hunter College of the City University of New York, New York, New York 10065, USA*
[2]*Graduate Center of the City University of New York, New York, New York 10016, USA*
[3]*Lawrence Livermore National Laboratory, Livermore, California 94550, USA*
[4]*Michigan State University, East Lansing, Michigan 48824, USA*
[5]*National Superconducting Cyclotron Laboratory, East Lansing, Michigan 48824, USA*
[6]*McClellan Nuclear Research Center–UC Davis, McClellan, California 95652, USA*
[7]*University of Alabama at Birmingham, Birmingham, Alabama 35294, USA*
[8]*University of Notre Dame, Notre Dame, Indiana 46556, USA*
[9]*University of Missouri, Columbia, Columbia, Missouri 65211, USA*
[10]*University of California, Berkeley, Berkeley, California 94720, USA*

(Received 8 September 2020; revised 22 November 2020; accepted 19 January 2021; published 26 February 2021)

Isotope harvesting is a method of collecting the long-lived radioisotopes that build up during the operation of ion-beam facilities in a way that is useful for subsequent research. As a demonstration of this method for the collection of a group IV metal at a fragmentation facility, the high-energy ^{88}Zr secondary beam produced from a 140-MeV/u ^{92}Mo primary beam at the National Superconducting Cyclotron Laboratory (NSCL) was stopped in a water target. The setup aimed to mimic the aqueous beam dump that will be implemented at the Facility for Rare Isotope Beams (FRIB). The collected ^{88}Zr and accompanying ^{88}Y decay daughter were radiochemically extracted from the solution and made into target samples suitable for neutron-capture cross-section measurements. These samples were then irradiated at two reactor facilities, and the ^{88}Zr average thermal-neutron-capture cross section (σ_T) and resonance integral (I) were determined to be $\sigma_T = (8.04 \pm 0.63) \times 10^5$ b and $I = (2.53 \pm 0.28) \times 10^6$ b. The σ_T value agrees well with previous results and I, determined for the first time here, was found to be the largest measured resonance integral by two orders of magnitude. The ^{88}Y thermal-neutron-capture cross section was determined to be less than 1.8×10^4 b. This work demonstrates the steps needed to make cross-section measurements with samples produced via aqueous isotope harvesting.

DOI: 10.1103/PhysRevC.103.024614

I. INTRODUCTION

Long-lived radionuclides are produced and accumulate at various locations within an accelerator during routine operation. Isotope harvesting [1] is the collection and purification of these byproduct radionuclides for use in subsequent research. Initial uses of this method have shown great promise to complement the conventional methodologies. At the Paul Scherrer Institute (PSI) in Switzerland, the copper beam dump that had been used during high-energy proton irradiations was dissolved, and the ^{60}Fe ($t_{1/2} = 2.62 \times 10^6$ yr) present was radiochemically separated from the mixture. A sufficiently pure amount of ^{60}Fe was isolated [2] to measure its half-life [3–5] and neutron-capture cross section [6,7], and to produce a set of standards for accelerator mass spectrometry [8]. In addition, numerous other isotopes are being pursued from the copper beam dump [9], irradiated graphite targets [10], and stainless steel parts [11] at PSI.

The implementation of isotope harvesting at the upcoming Facility for Rare Isotope Beams (FRIB) at Michigan State University (MSU) has attracted considerable interest because of the large quantities of a broad range of radioisotopes that will be produced during routine operation. At FRIB, a water-filled beam dump will be utilized to stop the primary beam and much of the beam-fragment distribution, opening up new opportunities to collect radioisotopes sought after in areas of nuclear science ranging from national security to medicine. Thus, in preparation for an extensive isotope-harvesting program at FRIB, there have been several efforts to investigate the efficacy of extracting radioisotopes deposited in a water target [12–16].

Initial efforts at the National Superconducting Cyclotron Laboratory (NSCL), which produces radioisotopes using the same fragmentation process as at FRIB, albeit at significantly lower intensities, demonstrated the successful recovery of ^{24}Na and ^{67}Cu from an aqueous target [12–14]. Both sodium and copper are well suited for collection and extraction from an aqueous environment; these elements have well understood redox and speciation chem-

*Corresponding author: js7294@hunter.cuny.edu

istry in near neutral environments, only exist as monovalent and divalent cations in solution, and do not hydrolyze irreversibly.

Other elements, such as Zr, V, and Hf, present challenges. These group IV and V metals tend to exist in tetravalent and pentavalent oxidation states, and form oxide and hydroxide complexes in aqueous conditions that are not highly acidic. This effect is most pronounced when metal concentrations exceed the micromolar regime [17]; however, even at trace concentrations, such as those expected for radioisotopes, mononuclear hydroxide complexes can form. Recent results have indicated a reduced recovery efficiency for ^{48}V deposited in an aqueous solution at the NSCL, potentially due to redox and radiolysis chemistry [15]. The work presented here is the first aqueous harvesting collection of a group IV element, and the efficacy of the method for collection of a hydrolyzable metal is assessed.

Several radioactive Zr isotopes are valuable to nuclear science, including ^{86}Zr and ^{89}Zr for nuclear medicine [18,19], ^{95}Zr for astrophysics [20], and ^{88}Zr and ^{89}Zr for stockpile-stewardship applications. For example, ^{88}Zr is part of a neutron-induced reaction network that is of interest for interpreting data from radiochemical detectors used in underground nuclear tests [21]. The daughter of ^{88}Zr, ^{88}Y, is also part of this network as well as of interest to the astrophysical community for *p*-process investigations [22]. Analysis of historic test data using such cross sections is an aspect of the United States' Science-Based Stockpile Stewardship Program, which aims to provide high confidence in the safety, security, reliability, and effectiveness of the nuclear stockpile without nuclear testing [23]. The only measurements of a neutron-induced reaction on ^{88}Zr were of the ^{88}Zr$(n, 2n)^{87}$Zr cross section at 14.8 MeV [24] and the thermal neutron-capture cross section on ^{88}Zr recently measured using samples produced via the ^{89}Y$(\mathrm{p}, 2n)^{88}$Zr reaction. The latter result revealed that the thermal-neutron-capture cross section on ^{88}Zr is $(8.61 \pm 0.69) \times 10^5$ b, which is the second largest reported neutron-capture cross section [25]. Similarly, the ^{88}Y$(n, 2n)^{87}$Y was measured at 14.8 MeV [24], and recent efforts have aimed to constrain the neutron-capture cross section on ^{88}Y from 0.01 to 1 MeV using the Oslo method [22].

In the work presented here, a secondary beam of ^{88}Zr was collected in the water target irradiation cell of an aqueous harvesting end station [12] at the NSCL in a dedicated experiment. While most harvesting efforts at FRIB will be carried out continuously without interfering with a users' experiment, dedicated experiments for proof-of-concept work at NSCL are useful to validate methodologies for both production and separation. The steps needed to extract and purify the ^{88}Zr produced via aqueous harvesting for a subsequent neutron-capture cross-section measurement were demonstrated. The aqueous samples were subsequently shipped to Lawrence Livermore National Laboratory (LLNL) for radiochemical separations and preparation of ^{88}Zr and ^{88}Y targets for measurements of thermal-neutron-capture cross sections. The targets were irradiated at two nuclear reactors, the University of Missouri Research Reactor (MURR) and the McClellan Nuclear Research Center (MNRC), to perform measurements of the neutron-capture cross sections. The measurements served to reproduce the recent ^{88}Zr neutron-capture results [25] and to better discern the relative contribution of thermal versus resonance region neutrons. While aqueous harvesting efforts at the NSCL have successfully demonstrated collection and purification of several radionuclides [12–15], the present effort is the first to utilize an aqueous harvested radionuclide for a subsequent measurement.

The methods developed for purifying Zr from the co-produced fragmentation products and harvesting matrix can be adapted to yield multiple useful samples once FRIB is online. Based on the expected production rates at FRIB, approximately 630 mCi of ^{88}Zr ($t_{1/2}$ = 83.4 d) will be made per week running with a full-intensity ^{92}Mo primary beam [1]. Given the notoriously complex speciation of Zr at near-neutral *p*H [26] and irradiation restrictions (e.g., minimal organic content and residual fluoride) on the final ^{88}Zr target material, the efficacy and efficiency of Zr recovery chemistry post-aqueous harvesting is important to assess.

II. AQUEOUS ISOTOPE HARVESTING OF ^{88}Zr AT NSCL

At the NSCL, a 10 pnA, 140-MeV/u ^{92}Mo primary beam impinged upon a 446-mg/cm^2 beryllium target to produce a range of fragmentation products. The A1900 projectile-fragment separator [27,28] was used to select the ^{88}Zr secondary beam for delivery to the irradiation cell. The overall beam composition was measured periodically throughout the run at the A1900 via the particle identification detector (PID), which characterizes the beam components by energy-loss and time-of-flight measurements of the individual ions. By adjusting the settings of the dipole magnets and mass slits of the separator, a momentum acceptance of 1.36% was achieved, which yielded the typical beam composition summarized in Table I.

The beam current was continuously measured using a nonintercepting beam monitor which provided a signal proportional to the electromagnetic field produced by the beam. To normalize this signal, direct measurements of the beam current were obtained regularly throughout the run both from a Faraday cup (FC), briefly inserted into the beam path immediately upstream of the endstation, and from the activity deposited in a graphite puck, positioned in front of the irradiation cell window for 5 minutes between each water target irradiation. The radioactive species collected in these $\frac{1}{2}$-inch-thick graphite pucks were quantified within 1 hour using a high-purity germanium (HPGe) γ-ray detector. It was assumed that the activities in the puck were representative of the beam composition and that nuclear reactions with the carbon did not substantially contribute to the observed products. The radionuclides detected in the puck are compared in Table I to the distribution of isotopes detected at the A1900. These two diagnostics indicated that ^{88}Zr was the most prevalent species in the beam, and overall gave consistent results, although the stable isotopes could not be quantified with γ-ray spectroscopy. This beam calibration indicated that the average rate of ^{88}Zr impinging upon the irradiation cell was 1.1×10^7 pps. Therefore, over the course of 6.1 days, $(5.8 \pm 0.4) \times 10^{12}$ atoms (corresponding to 15.0 ± 1.0 μCi) of ^{88}Zr were delivered to the cell.

TABLE I. Beam composition observed at the A1900 Particle Identification Detector and in the graphite puck. The radionuclide composition of the beam in the puck was determined from the emitted γ rays after a 5-min irradiation. The rates in atoms/s were inferred from the observed activities, after correcting for decay losses, and accounting for the puck irradiation time. For both the PID and the puck, the intensity of each radionuclide has also been listed normalized to ^{88}Zr.

Nuclide	Half-Life	PID atom %	Puck (atoms/s)	PID norm. to ^{88}Zr	Puck norm. to ^{88}Zr
^{91}Nb	680 yr	0.35%		0.007	
^{90}Nb	14.60 h	15.28%	1.28×10^7	0.316	0.394
^{89}Nb	2.03 h	0.20%		0.004	
^{89}Zr	78.41 h	4.76%	3.44×10^6	0.099	0.106
^{88}Zr	83.4 d	48.33%	3.26×10^7	1.000	1.000
^{87}Zr	1.68 h	0.31%	2.26×10^5	0.006	0.007
^{86}Zr	16.5 h		9.24×10^4		0.003
^{87}Y	79.8 h	14.50%[a]	1.12×10^6	0.300[a]	0.034
^{87m}Y	13.37 h		7.65×10^6		0.235
^{86}Y	14.74 h	9.91%[a]	2.44×10^6	0.205[a]	0.075
^{86m}Y	47.4 min		2.23×10^6		0.068
^{85}Y	2.68 h		3.45×10^5		0.011
^{84}Y	39.5 min		1.72×10^5		0.005
^{86}Sr	Stable	0.32%		0.007	
^{85}Sr	64.849 d	4.94%		0.102	
^{84}Sr	Stable	0.43%		0.009	
^{81}Sr	22.3 min		3.69×10^4		0.001
^{84}Rb	32.82 d	0.33%		0.007	
^{83}Rb	86.2 d	0.25%		0.005	
^{82}Rb	1.2575 min	0.09%		0.002	
^{81}Rb	4.572 h		2.39×10^5		0.007

[a]The PID did not distinguish between the isomer and ground state, so both contributions are reported as ground state.

The ^{88}Zr beam entered the water-filled irradiation cell by passing through a gold-vapor-deposited titanium window. To minimize chemical interactions, the cell walls were made of PEEK (polyether ether ketone) and the Au side of the window, which consisted of a 0.15-μm-thick layer of Au on a 75-μm-thick Ti foil, was in contact with the water. Prior to irradiation, the double-distilled water (OmniTrace® Ultra) in the irradiation cell was sparged with atmospheric pressure helium gas. After beam was deposited in the irradiation cell for an extended period of time, typically ranging from 10 to 16 hours, the water was transferred to an acid-washed PTFE (polytetrafluoroethylene) bottle. Following irradiation, the water was measured to be *p*H 5; each sample was acidified with 3 M HCl to decrease the *p*H to about 1.5, in an effort to minimize Zr hydrolysis. In total, ten bottles, each with 100 ml of irradiated water, were collected over the course of the experiment.

After each irradiation, the bottle of water was removed from the end station and the radioisotope content was analyzed using a HPGe detector in an analogous way as with the pucks. A typical γ-ray spectrum is shown in Fig. 1. The ^{88}Zr activity was characterized with the detection of its characteristic 392.87-keV γ ray (emitted with a γ-ray intensity $I_\gamma = 97.29\%$) [29]. A large number of other radioisotopes were also present in the water sample, with the spectrum dominated by the intense γ rays from the decays of the short-lived products ^{90}Nb and ^{86}Y. Radionuclides detected in the puck were also consistent with those collected in the water samples with the exception of ^{83}Sr, which was only detected in the water, due to its relatively low yield and the short irradiation time for the puck. The presence of 514-keV γ rays emitted following the decay of ^{85}Sr could not be detected in the pucks or the water samples immediately after bombardment because it was obscured by the annihilation radiation, but it was identified once much of the shorter-lived activity contributing to the annihilation peak reduced in intensity after several weeks of decay. The presence of some short-lived activities was reduced in the water relative to the puck as a results of decay during irradiation. The total activity of ^{88}Zr collected in the bottles was 9.6 ± 0.9 μCi at the end of all the collections, consisting of about 60% of the total ^{88}Zr delivered to the irradiation cell. Eight of the bottles, containing a total activity of 9 μCi of ^{88}Zr, were sent to LLNL for chemical processing. The two bottles from the shortest collections remained at MSU for small-scale chemistry tests.

Following the last collection, the empty irradiation cell was disassembled and the window removed so that the activity retained on these pieces could be assessed. Autoradiography of the cell and window was performed, and the image-plate results following a 16-hour exposure time are shown in Fig. 2. The autoradiograph of the window shows a clear image of the beam spot as well as where the water had been in contact with the window. The autoradiograph of the backplate of the cell similarly shows where the water had been in contact with the PEEK and splash marks from when the water had been transferred from the cell to the PTFE bottles.

γ-ray spectroscopy of the irradiation cell and window indicated that they had about 5.9 ± 0.2 and 0.5 ± 0.04 μCi of ^{88}Zr adsorbed, respectively. Together, these quantities accounted for the remaining 40% of the delivered ^{88}Zr activity. The ^{88}Zr

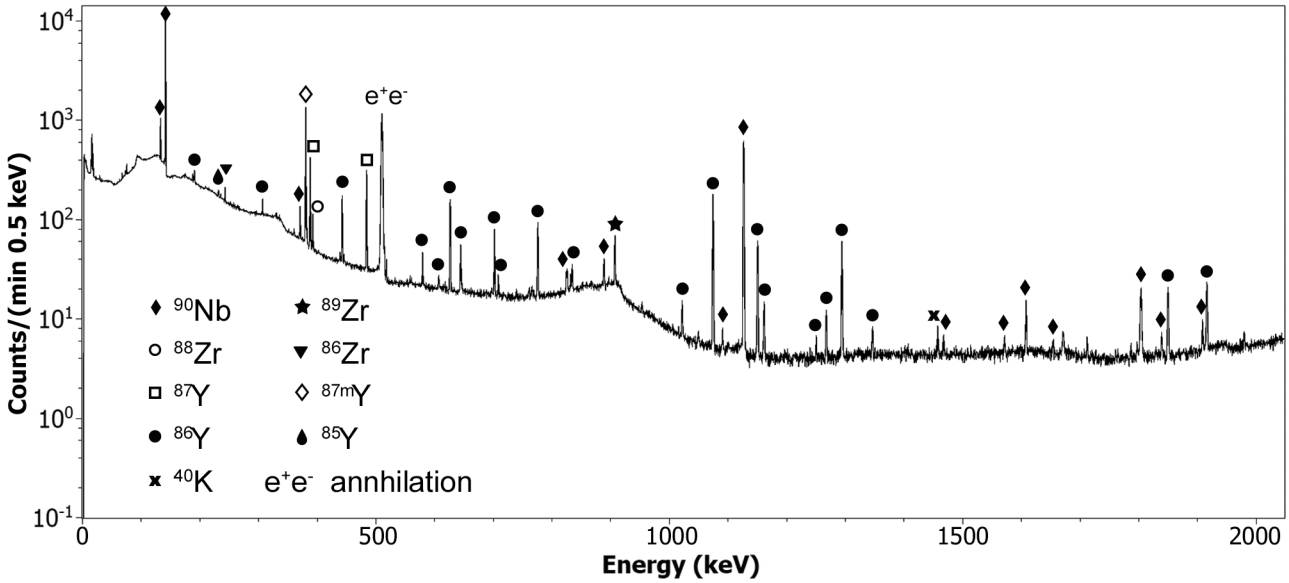

FIG. 1. γ-ray spectrum from a typical bottle containing an aqueous sample recorded 7 hours after being collected at the NSCL. Decay and efficiency corrections have not been applied. In addition to ^{88}Zr, many other ^{92}Mo fragmentation products are observed, including ^{90}Nb, ^{87m}Y, and ^{86}Y.

activity on the backplate is about 12 times that observed on the window; this is not purely due to the surface area exposed to the water, which would account for approximately a factor of 4. It is not clear why the Zr adsorbed to the PEEK to such a high degree, but it is possible that a hydrolyzed Zr species coordinated with the ketone moieties of the PEEK surface. In addition, $^{87/87m}$Y, ^{89}Zr, ^{86}Y, and ^{90}Nb were also adsorbed. By the time the spectra were collected on the cell and window, nearly all of the ^{87}Zr ($t_{1/2}$ = 1.68 h) had decayed to $^{87/87m}$Y. It is assumed that the higher localization of $^{87/87m}$Y activity on the cell and window rather than in the water is a result of this decay. This is similarly the case with ^{86}Y, produced from the decay of ^{86}Zr.

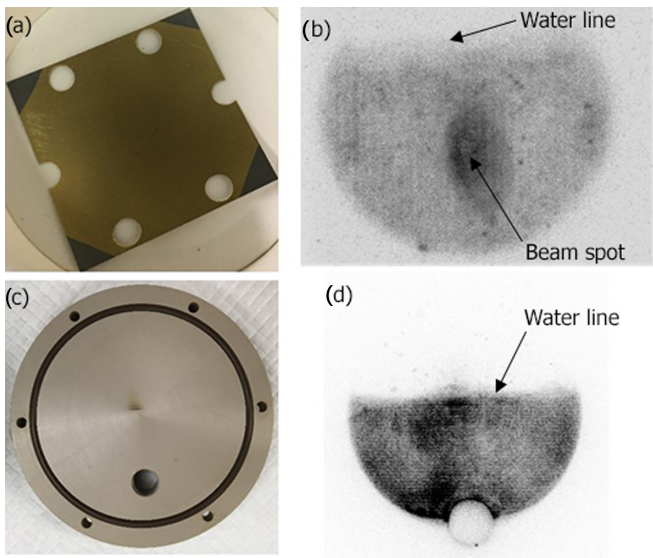

FIG. 2. (a) photograph of the gold-vapor-deposited titanium entrance window to the cell prior to irradiation, (b) autoradiograph of the window after irradiation, (c) photograph of the backplate of the cell after irradiation, and (d) autoradiograph of the backplate of the cell after irradiation. In (b) and (d), the darker areas indicate locations with higher radioactivity. The cell backplate, which was in contact with the water of the cell, contains about 12 times the radioactivity of the entrance window.

III. RADIOCHEMICAL PROCESSING AND TARGET FABRICATION

The eight bottles received at LLNL had a total of 800 ml of dilute HCl. The radiochemical processing was performed about one month after the sample collection, and at that time the samples contained approximately 7 μCi, or 0.4 ng, of ^{88}Zr as well as about 1.1 μCi, or 0.1 ng, of ^{88}Y resulting from ^{88}Zr decay. Most of the other radioisotopes have half-lives short enough that they had decayed away, with only ^{85}Sr and ^{83}Rb still present in the sample in detectable amounts. Of the eight bottles, six were radiochemically processed to purify ^{88}Zr and ^{88}Y to serve as target materials for neutron-capture cross section measurements.

The overall chemistry flowchart used to isolate the ^{88}Y and ^{88}Zr samples is shown in Fig. 3. The ^{88}Y and ^{88}Zr needed to be concentrated into a smaller volume and separated from one another, which was done using cation exchange and coprecipitation followed by anion exchange, respectively. Previous work successfully demonstrated separations of ^{88}Zr from stable Y target material using anion exchange chromatography [25]. However, as a result of the large volume of solution generated during aqueous harvesting, a preconcentration step was required for these samples. Evaporating the water samples for preconcentration, as had been done in previous aqueous harvesting experiments [12,15], resulted in ^{88}Zr irreversibly adsorbed to the polypropylene tubes. Therefore, various

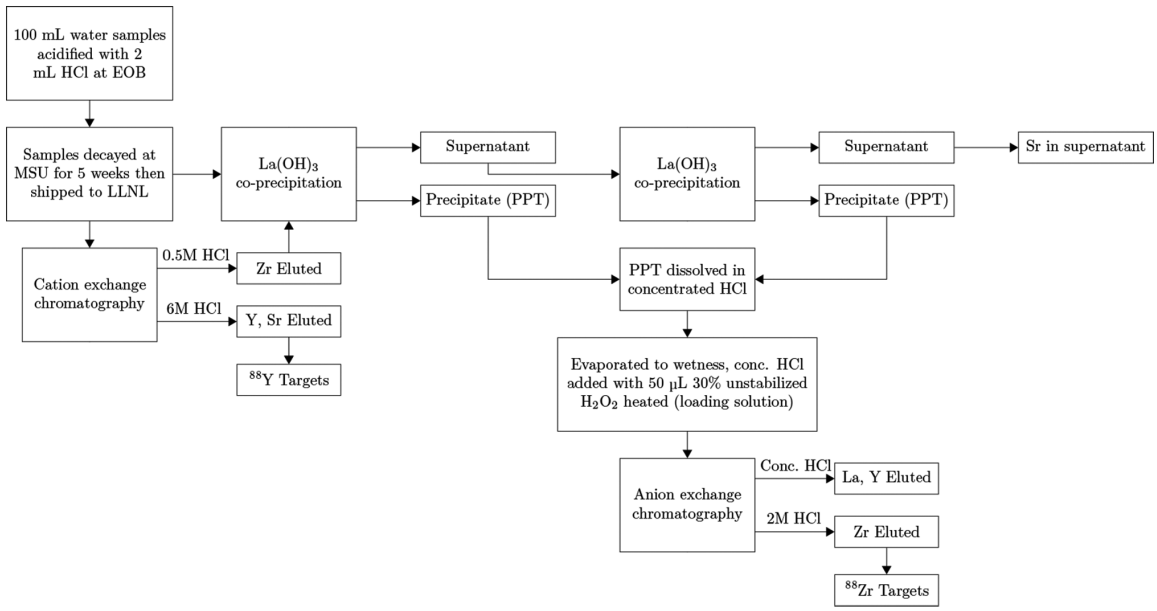

FIG. 3. Flowchart depicting the steps taken to isolate ^{88}Zr and ^{88}Y from the harvested samples for target production.

preconcentration and separation techniques were tested, with the highest recovery (≈70%) coming from coprecipitation of the ^{88}Zr using $La(OH)_3$ followed by anion exchange. Stable Zr carrier could not be added as this would interfere with the subsequent neutron irradiation.

Given the low mass of Zr, coprecipitation with La was done via hydroxide precipitation with NH_4OH, which carries both the Zr and the Y. To minimize the total mass of La introduced, 4 mg of La^{3+} were used by iteratively coprecipitating $2 \times$ 20 ml aliquots of the NSCL collections with 1 mg La^{3+} in each tube. The precipitated mixture was centrifuged at 4000 rpm for 5 minutes and the supernatant removed. The precipitate was dissolved in concentrated HCl and the next 20 ml of the sample solution added, repeating the precipitation procedure. The supernatants were spiked with an additional 1 mg of La carrier and precipitated, centrifuged, and separated again. The precipitates from each of the two passes were dissolved in concentrated HCl and combined. This coprecipitation process successfully concentrated greater than 95% of the ^{88}Zr from the aqueous samples.

The dissolved $La(OH)_3$ precipitate from the preconcentration step was evaporated to wetness and additional concentrated HCl added with a couple of drops of 30% unstabilized H_2O_2 (≈50 μl), which helped keep Zr in solution. The stock was heated briefly to destroy the peroxide prior to loading on Dowex 1X8 (100–200 mesh, 1 cm × 7 cm, column volume (CV) ≈ 5 ml) strong-base anion exchange resin that was preconditioned with concentrated HCl. After adding the loading solution (≈2.5 ml), the resin was washed with 6 CVs of concentrated HCl to elute the Y and La. The Zr was eluted with 2 M HCl in 5 CVs. Likely as a result of hydrolysis of the Zr upon stopping in the water during irradiation, it adhered to the polypropylene containers used for chemistry, which otherwise would typically have low Zr retention. Desorption of the Zr was attempted with a variety of matrices with the most successful being a mixture of hot concentrated HCl and a few drops of 30% unstabilized H_2O_2, added to the resin while still warm. This, however, was only done as a final desorption attempt as the hot HCl/H_2O_2 destroys the resin. The overall chemistry recovery of the ^{88}Zr was just over (26 ± 2)% after the full chemical processing summarized in the flowchart in Fig. 3. The ^{88}Zr in 2 M HCl was concentrated to about 100 μl to make the targets.

The low recovery of ^{88}Zr is largely attributed to hydrolysis of the Zr. When the beam initially stops in the water cell, the water is approximately *p*H 5. The ions collected in the cell were at this *p*H for 10–20 hours. After the irradiation, the water was acidified with HCl to approximately *p*H 1.5, but at this point irreversible species seem to have already formed. At *p*H 5 with dilute Zr concentrations ($[Zr] < 10^{-6}$ M), the dominant speciation for Zr is its hydrolyzed form $Zr(OH)_4$ [30]. At *p*H 1.5, that species is a more minor constituent with $Zr(OH)_3^+$ and $Zr(OH)_2^{2+}$ dominating. The post-irradiation counting of the irradiation cell and its window indicated that just over one third of the ^{88}Zr produced was sorbed to these materials, as opposed to collected in the water samples. This is indicative of hydrolysis of the Zr causing it to adhere to both the gold and PEEK surfaces.

The precipitation of the Zr has high recovery as it was done in a hydroxide precipitate that would carry any of the aforementioned Zr species. These species, however, behave differently chromatographically from Zr^{4+}, as they cannot form the $Zr(Cl)_6^{2-}$ anionic complex. Further, the hydrolyzed species are susceptible to adhering to surfaces through strong electrostatic interactions that inhibit their recovery. This was observed during separation chemistry, in which portions of the Zr adhered to the polypropylene centrifuge tubes and chromatography columns. The bulk of the ^{88}Zr that was not recovered during chemistry was lost to the polypropylene centrifuge tubes, despite various attempts at desorption.

It is expected that Zr recovery will improve if the beam is stopped in more acidic solutions to minimize hydrolysis

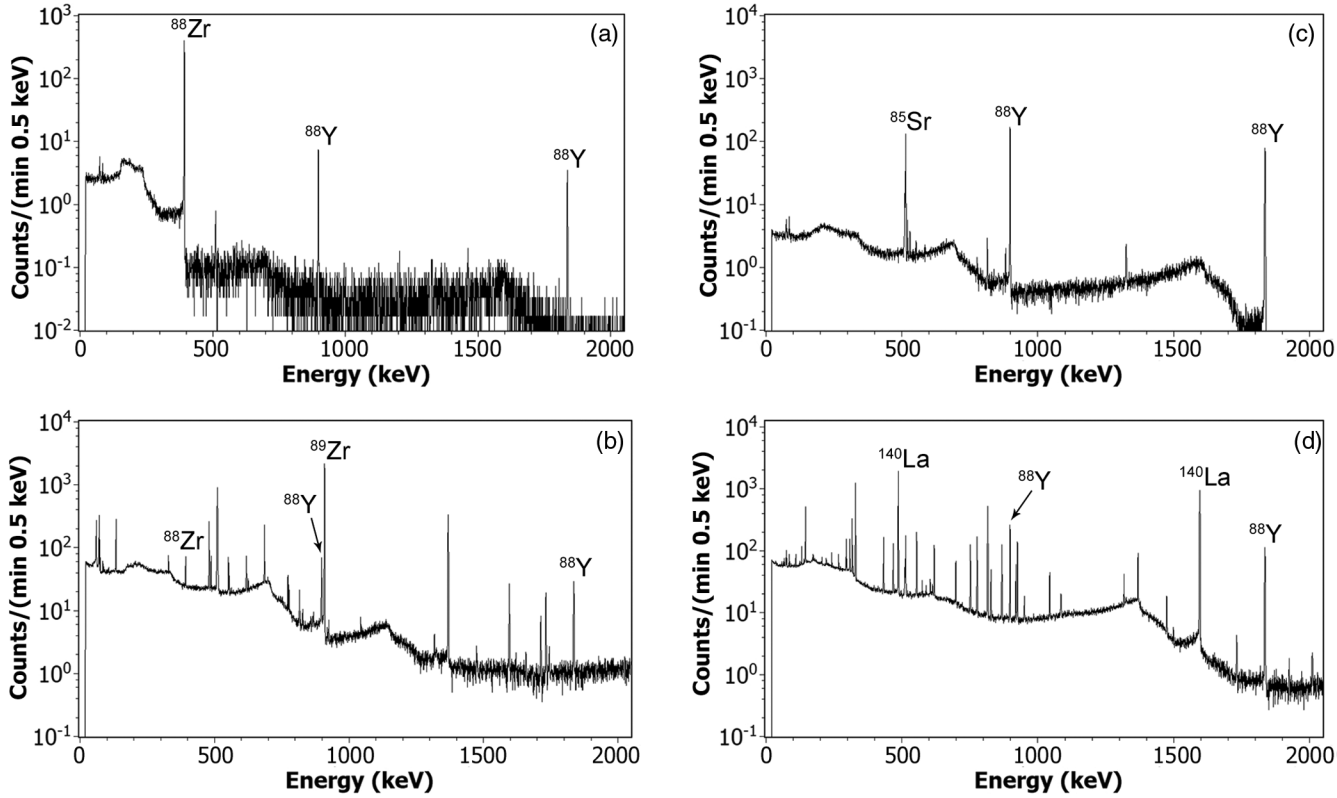

FIG. 4. γ-ray spectra of (a) ^{88}Zr target before irradiation, (b) ^{88}Zr target after 10-hour irradiation at MURR and 3.6-day decay, (c) ^{88}Y target before irradiation, and (d) ^{88}Y target after 10-hour irradiation at MURR and 7.4-day decay. Decay and efficiency corrections have not been applied. The initial ^{88}Zr activity was accompanied by ^{88}Y, which grew in from the decay following chemical separation. After irradiation, the ^{88}Zr activity was greatly reduced and a large quantity of ^{89}Zr was present. Conversely, no ^{88}Y burnup was observed in the ^{88}Y targets after irradiation. The initial ^{88}Y activity was accompanied by ^{85}Sr and a small amount of ^{83}Rb. After irradiation, ^{140}La, the radiative capture product on stable ^{139}La, was also observed.

potential or with the addition of strong complexants such as fluoride which form stronger complexes than hydroxide. The water-filled beam dump at FRIB will operate at or near neutral *p*H, in part due to the logistical challenges of executing such an experiment with highly acidic and potentially corrosive matrices. Therefore, future studies will explore alternative collection methods for hydrolyzable radioactive beam fragments.

The ^{88}Y present in two of the collection bottles was isolated prior to recovering the ^{88}Zr. The solutions from these two bottles were passed through 50WX8 cation exchange resin (100–200 mesh, 0.8 cm $\times$ 2 cm) that had been preconditioned with 0.5 M HCl. The resin was rinsed with 0.5 M HCl, eluting the Zr. During loading and rinsing, the Y was retained on the resin along with most of the Sr, while the Zr was collected as an eluate for use in the precipitations. The Y was then eluted with 6 M HCl and concentrated to make the ^{88}Y stock for target preparation. After separation, 80% of the ^{88}Y was concentrated as the final Y stock, which had no detectable ^{88}Zr. The Y stock contained 0.9 μCi of ^{88}Y, 0.3 μCi of ^{85}Sr, and 0.02 μCi of ^{83}Rb, which were not further separated because the ^{85}Sr and ^{83}Rb do not interfere with the ^{88}Y$(n,\gamma)^{89}$Y measurement.

Two ^{88}Y and four ^{88}Zr targets were prepared by pipetting the respective stocks into 4 mm $\times$ 6 mm (inside diameter $\times$ outside diameter) Suprasil quartz tubes that had been flame sealed on one end. The Y and Zr in HCl deposits were dried in a water bath evaporator with nitrogen flowed into the tubes. After drying, the tubes were flame sealed and leak tested. A portion of the ^{88}Y and ^{88}Zr stocks was set aside for characterization.

The stable element content in the samples was determined with inductively coupled plasma-mass spectrometry (ICP-MS) by analyzing aliquots consisting of 100 μl of the ^{88}Y and ^{88}Zr stocks that had been diluted to 5 ml with 2% HNO_3. In the ^{88}Zr targets, the stable Sr, Y, Zr, Nb, Mo, and La contents were found to be in the ranges 0.79–2.3 ng, 0.03–0.07 ng, 27–79 ng, 0.4–1.1 ng, 6.2–18 ng, and 0.03–0.09 ng, respectively. In the ^{88}Y targets, the stable Sr, Y, Zr, Nb, Mo, and La contents were found to be in the ranges 15–25 ng, 0.94–1.6 ng, 5.5–9.0 ng, 0.02–0.03 ng, 1.4–2.4 ng, and 18–29 ng, respectively. Despite the La carrier initially being present at nearly 10^9 times the ^{88}Zr mass (7.4×10^{-12} g) after coprecipitation, it was successfully separated with a decontamination factor of 10^8. The stable element content in each sample was low enough that it did not interfere with the subsequent cross-section measurements. For stable Zr content, this was demonstrated with the Zr monitors. For the 60 mg Zr monitor, ^{89}Zr activity produced via the ^{90}Zr$(n,2n)^{89}$Zr reaction was less than 10% of that observed in the coirradiated ^{88}Zr samples. With 10^{-6}

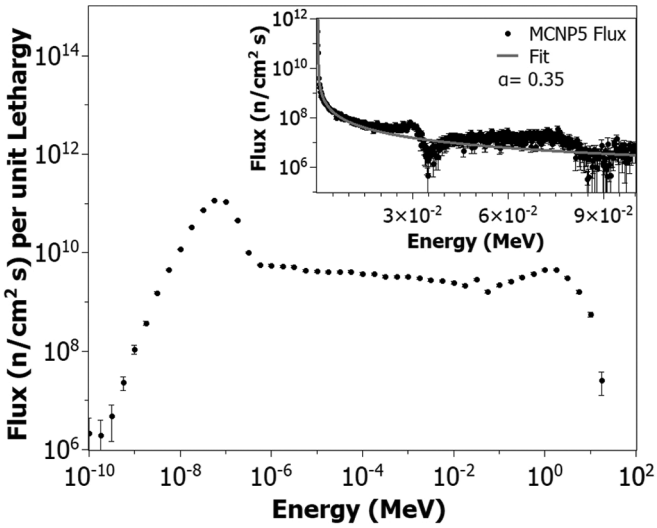

FIG. 5. Neutron energy spectra of MNRC reactor in NTD void location calculated using MCNP5. The main figure displays the full energy range on a logarithmic scale with lethargy-normalized flux. The inset features a more detailed model of the epithermal region on a linear energy scale with the non-normalized flux. More points were used to model this region to allow for a fit (gray solid line) to determine the epithermal-neutron shape factor. Both calculations include the 1-cm-thick Al sample holder.

times less stable Zr present in the ^{88}Zr sample, the percent contribution of ^{89}Zr from this source is negligible. Here the stable Zr content did not impact the subsequent cross-section measurements; however, this will have to be assessed on a reaction-by-reaction basis for future measurements.

The sealed samples were characterized with γ-ray spectroscopy to assess the initial amounts of each radionuclide. The γ-ray spectrum of a typical ^{88}Zr target is shown in Fig. 4(a). Although the yield of the chemistry was only 26%, the radiopurity of the ^{88}Zr sample was high; the only other radionuclide present in the ^{88}Zr targets was its decay daughter, ^{88}Y, which grew in after the ^{88}Zr separation. At the end of separation, the atom ratio of ^{88}Zr to ^{88}Y was on the order of 10^3. A typical γ-ray spectrum from a ^{88}Y target is shown in Fig. 4(c). The dominant species are ^{88}Y and ^{85}Sr. Other minor features in the spectrum are escape peaks from the 1836.063-keV γ ray from the decay of ^{88}Y, the 511-keV annihilation peak, and the photopeaks due to the decay of ^{83}Rb.

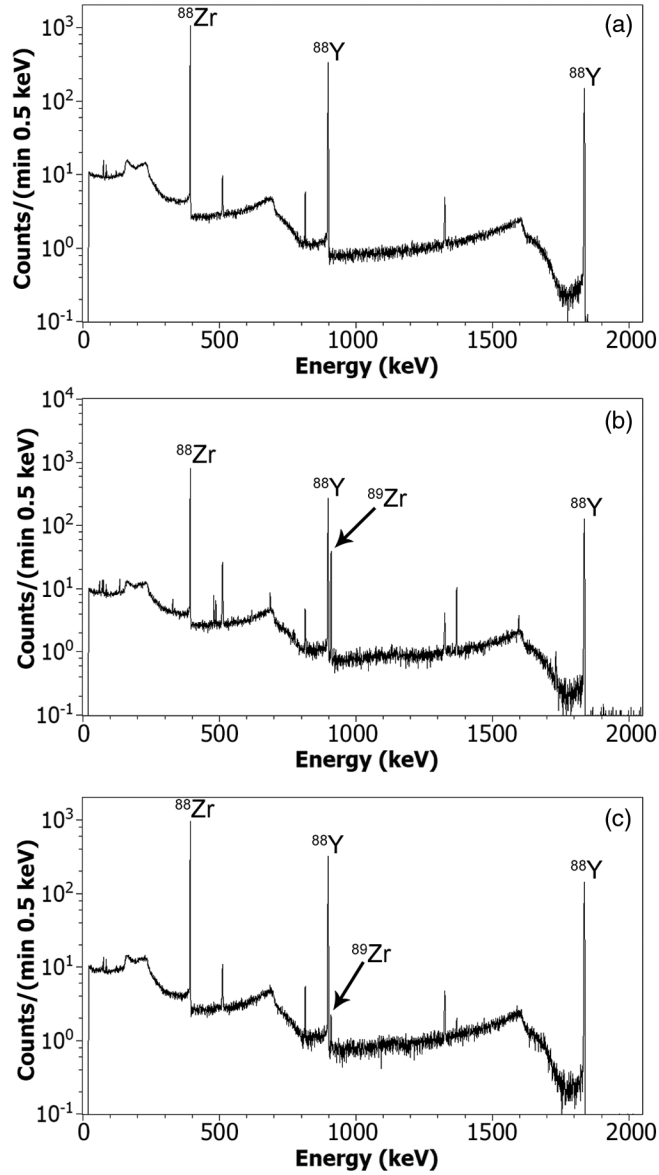

FIG. 6. Typical γ-ray spectra of a ^{88}Zr target (a) before irradiation, (b) after irradiation at MNRC, and (c) after irradiation at MNRC in a Cd-lined container. Decay and efficiency corrections have not been applied. The initial target contained only ^{88}Zr and its daughter ^{88}Y, and after irradiation a decrease in the ^{88}Zr and an increase in the ^{89}Zr were observed. When the thermal-neutron flux was suppressed with the Cd liner, the ^{88}Zr burnup and ^{89}Zr production were both reduced.

TABLE II. Summary of characteristics for each target used for subsequent neutron irradiation.

Target No.	Radionuclide	Activity at beginning of irradiation (kBq)	Irradiation time (h)	Irradiation facility	Cadmium covered
1	^{88}Zr	3.31 ± 0.11	1	MURR	No
2	^{88}Zr	3.63 ± 0.12	10	MURR	No
3	^{88}Zr	3.81 ± 0.12	12	MNRC	No
4	^{88}Zr	4.68 ± 0.19	12	MNRC	Yes
5	^{88}Y	7.17 ± 0.30	1	MURR	No
6	^{88}Y	4.34 ± 0.18	10	MURR	No

TABLE III. Measured thermal and resonance region neutron flux from MURR and MNRC determined from the Fe, Zr, and Mo flux monitors irradiated alongside the ^{88}Zr and ^{88}Y samples. The average flux was determined from three or four neutron-capture reactions with known cross sections depending on whether a Mo foil was included.

		Measured average flux (n/cm^{2}s)			
Sample	Irradiation time (h)	Thermal	Resonance	Thermal/resonance	Monitor foils
MURR	1.0	$(7.71 \pm 0.46) \times 10^{13}$	$(2.33 \pm 0.22) \times 10^{12}$	33	Fe, Zr, Mo
MURR	10.2	$(8.05 \pm 0.50) \times 10^{13}$	$(2.30 \pm 0.22) \times 10^{12}$	35	Fe, Zr
MNRC	12.0	$(2.54 \pm 0.15) \times 10^{11}$	$(3.94 \pm 0.36) \times 10^{9}$	65	Fe, Zr, Mo
MNRC/Cd lined	12.0	$(1.55 \pm 0.17) \times 10^{9}$	$(2.86 \pm 0.26) \times 10^{9}$	0.54	Fe, Zr, Mo

IV. NEUTRON-CAPTURE CROSS-SECTION MEASUREMENTS

The cross sections were determined through the activation method using γ-ray spectroscopy to measure the burnup of the target and, in the case of ^{88}Zr, the production of the capture product after neutron irradiation. The samples were shipped to MURR and MNRC for irradiation (Table II).

At MURR, one set of samples was irradiated for 1 hour and a second one for 10 hours in the graphite reflector. Each set contained a ^{88}Zr sample, a ^{88}Y sample, and a collection of monitor foils individually encapsulated in quartz. The monitor foils for the 1-hour irradiation contained stable Zr, Fe, and Mo while the 10-hour set contained only Zr and Fe; Mo was not included in this set because of the high level of activity that would be produced.

After irradiation, the samples were removed from the reactor, extracted from the irradiation canister in a hot cell, and packaged for shipping. The samples were shipped back to LLNL and the exteriors cleaned with aqua regia and 18.2 MΩ cm water washes to remove any contamination. The samples were then opened and the residues dissolved with 9 M HCl ($\approx$ 500 μl), which were diluted with 18.2 MΩ cm water to 10 ml. Starting 3 days after the irradiation, these ^{88}Y and ^{88}Zr samples were counted for approximately 1 month to track the decay of the γ-ray lines shown in Figs. 4(b) and 4(d). The populations of ^{88}Zr, ^{89}Zr, and ^{88}Y atoms were determined from the intensity of the characteristic γ-ray peaks detected at 909.15, 392.87, and 898.042 keV, respectively [29,31]. The monitor foils were extracted from the quartz vial and individually counted to quantify the dominant activation products from the γ-ray peaks at energies listed in parentheses: ^{59}Fe (1099.245 and 1291.59 keV), ^{95}Zr (724.192 and 756.725 keV), ^{97}Zr (743.36 keV), and ^{99}Mo (181.068 and 739.5 keV).

At MNRC, two sets of samples containing ^{88}Zr and Fe, Zr, and Mo monitor foils separately encapsulated in quartz were irradiated for 12 hours in the Neutron Transmutation Doping (NTD) location. This location has the highest ratio of thermal (<0.5 eV) to fast (>1 MeV) neutrons in the MNRC reactor, with thermal and resonance region flux values determined from the monitor foils shown in Table III. The neutron flux in that location was modeled using MCNP5 (Fig. 5) to demonstrate the shape of the epithermal neutron region. The non-lethargy-normalized flux values obtained from MCNP5 were fit with the equation

$$\Phi_{ep}(E) = \Phi_{ep,c}\frac{(1eV)^{\alpha}}{E^{1+\alpha}} \quad (1)$$

where $\Phi_{ep,c}$ is a proportionality constant to determine the epithermal neutron shape factor, α [32]. For an ideal $1/E$ spectrum, α is 0, while we calculated a value for α of 0.35. It should be noted that this epithermal neutron shape factor determined from the model only describes the general shape of the spectrum, averaging out local features unique to the irradiation position.

One set of samples was irradiated with a 1-mm-thick cadmium wrapping, to reduce the thermal flux by about two orders of magnitude. After irradiation, the samples remained at MNRC for 2.5 days to allow the shortest-lived activities to decay away. They were then returned to LLNL where the exteriors were wiped clean and counted within 3 days following the irradiation. The monitor foils were counted in the same manner as the MURR samples. Typical γ-ray spectra of the samples before and after irradiation are shown in Fig. 6.

A. Thermal and resonance-region cross sections for ^{88}Zr

The ^{88}Zr and ^{89}Zr atom populations were quantified using their characteristic γ rays at 392.87 and 909.15 keV ($I_\gamma = 99.04\%$), respectively [29,31]. The 909-keV peak in the MURR-irradiated samples was found to decay with an average half-life of 3.27 ± 0.02 days, which agrees with the well-established value of 3.267 ± 0.005 d for the half-life of ^{89}Zr. The less intense transitions at 1657, 1713, and 1745 keV from the decay of ^{89}Zr were also observed. The 909-keV peak is clearly the result of ^{89}Zr decay based on the half-life and presence of multiple γ-ray lines.

The inferred number of ^{88}Zr and ^{89}Zr atoms was corrected for decay both during and after irradiation. While the decay during irradiation for ^{88}Zr is less than a 2% effect, the correction for ^{89}Zr is up to 6% for the 10-hour MURR irradiations. The measured ground state ^{89}Zr atoms originate from the decay of ^{89m}Zr, which is predominantly populated in the radiative-capture process due to angular-momentum considerations. The deduced number of ^{89}Zr atoms therefore has to be adjusted for the branching ratio of ^{89m}Zr, which decays by isomeric transition to the ground state 93.77% of the time [31]. The resulting ^{89}Zr population was then normalized to the initial ^{88}Zr population to adjust for differences in ^{88}Zr in each target. The thermal-neutron-capture cross section for ^{89}Zr was previously constrained to 1.2×10^4 b [25], which has been supported with recent nuclear data calculations [33]. Despite the large magnitude of the predicted and constrained cross section for ^{89}Zr, it is still 1.5% that of ^{88}Zr, and thus the

TABLE IV. Summary of 1σ uncertainty contributions for each aspect of the experiment. The final uncertainty on each measurement was assessed by weighting the listed contributions and assessing their impact on the central value. Correlated uncertainties were common across each measurement listed in Table II, while uncorrelated uncertainties varied from sample to sample.

Source of uncertainty	Magnitude	Correlated or uncorrelated
Chemical composition and yield		
Counting statistics	<3%	Uncorrelated
Sample geometry	3%	Uncorrelated
Point-source calibration of HPGe efficiency	1%	Correlated
Dilutions by mass	<0.5%	Uncorrelated
Mass spectrometry	0.5–10%	Uncorrelated
Neutron flux		
Monitor mass	0.3–7.4%	Uncorrelated
Irradiation time	<0.8%	Uncorrelated
Sample geometry	3%	Uncorrelated
Point-source calibration of HPGe efficiency	1%	Correlated
Counting statistics	<2%	Uncorrelated
Reference cross-section data, thermal	5.6%	Correlated
Reference cross-section data, resonance	8.8%	Correlated
Final-to-initial atom ratios		
Sample geometry	6%	Uncorrelated
Point-source calibration of HPGe efficiency	1%	Correlated
Counting statistics	0.5–4.6%	Uncorrelated

subsequent burnup of ^{89}Zr via radiative capture is a negligible loss mechanism within the uncertainty of this measurement.

The MNRC irradiation provided measurements with two different neutron-energy spectra, obtained with and without the thermal-neutron flux suppressed by a Cd absorber. From the results of these two irradiations, the thermal-neutron-capture cross section and resonance integral from ^{88}Zr were determined using methods described in Refs. [34–36]. The thermal and resonance-region neutron-flux values (Φ_T and Φ_{ep}, respectively) were determined from the monitor-foil reactions which have well known neutron-capture cross sections in these two energy regions [37]. The average neutron flux the samples were exposed to is presented in Table III. The unlined sample was exposed to a thermal-neutron flux over two orders of magnitude larger than the Cd-lined sample. The initial number of ^{88}Zr atoms [$N_{88}(0)$] in the unlined and Cd-lined samples, and the atoms of ^{89}Zr present after irradiation (N_{89}) were determined in the same way as with the MURR samples.

The cross sections for the thermal (σ_T) and resonance region (I) were extracted using the equation

$$N_{89}(\Phi) = N_{88}(0)[1 - e^{-t_i(\sigma_T \Phi_T + I\Phi_{ep})}], \quad (2)$$

where t_i is the irradiation time, which was the same for both irradiations. As the energies and widths of the ^{88}Zr resonances have not yet been measured, the reported value for I is uncorrected for $1/v$ behavior, as this cannot be assumed from the existing measurements.

Based on these measurements, the thermal-neutron-capture cross section and uncorrected resonance integral for ^{88}Zr$(n,\gamma)^{89}$Zr were determined to be $(8.81 \pm 0.63) \times 10^5$ b and $(2.53 \pm 0.28) \times 10^6$ b, respectively. While the resonance integral here was found to be a factor 3 greater than the thermal cross section, this ratio is in line with other I/σ ratios, especially for other isotopes near ^{88}Zr [37,38]. To the best of our knowledge, this resonance integral is the largest measured to date by a factor of 100 over the second largest, ^{155}Eu ($I = 2.32 \times 10^4$ b) [39]. Given the magnitude of the cross sections here and potential for unexpected behavior as a result of this, a further evaluation of resonance widths and locations is required to give a more complete picture of the resonance integral. The 1σ uncertainties here for the thermal-neutron-capture cross section and resonance integral are about 7% and 11%, respectively. The uncertainties in the results (Table IV) were driven by correlated contributions from the nuclear data of known cross sections for the monitor foil reactions used to determine the neutron flux. The main uncorrelated contribution was from the counting geometry uncertainty. Other minor uncertainty contributions arise from nuclear counting statistics, masses, irradiation times, and photopeak efficiencies. For the two samples sent to MURR, the thermal-neutron-capture cross section for ^{88}Zr (σ_T) was calculated from the production of ^{89}Zr using Eq. (2). The value for the resonance integral, I, determined from the MNRC measurement was used here. The thermal and resonance region neutron capture cross sections on ^{89}Zr were previously determined to be small relative to the ^{88}Zr values [25], and thus are neglected. The thermal-neutron-capture cross sections for ^{88}Zr$(n,\gamma)^{89}$Zr calculated from ^{89}Zr production for the 1-hour and 10-hour irradiations at MURR are $(8.55 \pm 0.63) \times 10^5$ b and $(7.78 \pm 0.59) \times 10^5$ b, respectively.

The thermal-neutron-capture cross section for ^{88}Zr was also determined from the disappearance of ^{88}Zr using

$$N_{88}(\Phi) = N_{88}(0)e^{-t_i(\sigma_T \Phi_T + I\Phi_{ep})}, \quad (3)$$

which is effectively the complement of Eq. (2). From the burnup of ^{88}Zr, the thermal-neutron-capture cross-sections for ^{88}Zr$(n,\gamma)^{89}$Zr were found to be $(8.40 \pm 0.63) \times 10^5$ b and $(6.99 \pm 0.55) \times 10^5$ b for the 1-hour and 10-hour irradiations, respectively. The average of the four

thermal-neutron-capture cross sections measured at MURR and the one measured at MNRC is $(8.04 \pm 0.63) \times 10^5$ b, where the uncertainties between the measurements are highly correlated and therefore are not reduced. The thermal-neutron-capture cross section can be compared with the previously measured value of $(8.61 \pm 0.69) \times 10^5$ b [25]. However, the analysis of the present work separately takes into account the contribution of the resonance integral and the thermal-neutron contribution whereas the previous result attributed all reactions to the thermal flux. The impact of including the resonance integral in an analogous way for the previous result reduces the thermal cross section by about 10%. Good agreement is obtained between the two sets of measurements.

B. Thermal neutron capture cross section ^{88}Y

The neutron-capture cross section for ^{88}Y is more difficult to determine because the reaction product, ^{89}Y, is stable. Therefore, with decay spectroscopy, the only available signature was a decrease in ^{88}Y activity following irradiation that exceeded that expected from radioactive decay. For the ^{88}Y samples, the characteristic γ-ray peaks at 898 and 1836 keV were prominent both before and after neutron irradiation. After accounting for decay losses, the number of ^{88}Y atoms remained constant within uncertainty following both the 1- and 10-hour irradiations at MURR. As such, a limit could be set for the cross section using Eq. (3) together with the estimate that the minimum detectable ^{88}Y burnup ($\frac{N_{88}(\Phi)}{N_{88}(0)}$) in the experiment is the 2σ uncertainty limited by the 3% geometric counting uncertainty. For this calculation, the resonance region contribution was not considered. Based on the data collected for the sample irradiated for 10 hours, an upper limit of 1.8×10^4 b was obtained for the thermal-neutron-capture cross section on ^{88}Y. This value is therefore at least 400 times smaller than that of ^{88}Zr, and further supports that the large ^{88}Zr neutron-capture cross section is not associated with the nearby $N = 50$ neutron-shell closure [25], as ^{88}Y is only one neutron away while ^{88}Zr is two neutrons away. The predicted neutron-capture cross section for ^{88}Y is 18.7 b [33], which falls well within the limit established here.

V. CONCLUSION

Aqueous harvesting was used to collect and purify ^{88}Zr from a mixture of ^{92}Mo fragmentation products that had been stopped in a water cell at the NSCL. The chemical recovery efficiency achieved for ^{88}Zr was (26 ± 2)%; however, the radiopurity was nearly 100% following chemical separation, with the only radioactive contaminant being the subsequent ingrowth of the ^{88}Y daughter. Previous experiments achieved greater recovery efficiencies for secondary beams of ^{22}Na [12] and ^{67}Cu [13,14], but challenges were encountered for ^{48}V [15] that were similar to what was encountered during this ^{88}Zr harvesting experiment. This set of experiments, although limited, seems to indicate that species that are readily hydrolyzed will be more difficult to efficiently collect via aqueous harvesting at FRIB in a water beam dump.

The accumulation of ^{88}Zr in a single aqueous sample lasted for up to 16 hours, giving ample time for even kinetically slow chemical processes to occur. Circulating the water in the FRIB beam dump directly into a chemistry setup [40] to minimize the time between irradiation and chemistry will likely help minimize the surface adsorption, especially for the kinetically slower processes. Recently, a hollow fiber supported liquid membrane (HFSLM) coated with the extractant Aliquat 336 was used to extract ^{48}V. This method was intended to simulate a circulating aqueous harvesting experiment and demonstrated an extraction efficiency of 71% for ^{48}V present at the part-per-trillion level in an aqueous matrix [41]. The addition of complexants or acids that interact with these metals to the circulating water may also allow for higher recovery efficiency.

Using an energetic charged-particle beam to produce ^{88,89}Zr from ^{89}Y in solution could induce a similar water radiolysis condition that may be aiding in the Zr hydrolysis and will also allow for shorter irradiations and kinetic studies [42,43]. Given that the group IV and V metals tend to hydrolyze above *p*H 1.5, future efforts targeting these species should focus on alternative harvesting methodologies, such as circulating aqueous systems, use of complexants, or transitioning to other phases of harvesting, such as implementation of solid collectors.

The results obtained from the MURR and MNRC irradiations of samples produced from the isotopes collected at the NSCL yielded a weighted average thermal-neutron-capture cross section for ^{88}Zr of $(8.04 \pm 0.63) \times 10^5$ b and an uncorrected resonance integral of $(2.53 \pm 0.28) \times 10^6$ b. In addition, an upper limit on the thermal neutron ^{88}Y$(n, \gamma)^{89}$Y cross section was established to be 1.8×10^4 b.

Despite the chemistry challenges, this work was the first demonstration of the sequence of steps needed to collect radioisotopes deposited in an aqueous target at a fragmentation facility and to use that material for subsequent cross-section measurements. The production rates of ^{88}Zr at FRIB are expected to reach approximately 3×10^4 times higher than at the NSCL and would yield about 630 mCi of ^{88}Zr per week. Additionally, new instruments such as the Device for Indirect Neutron Capture Experiments on Radionuclides (DICER) at the Los Alamos Neutron Science Center (LANSCE) could be used for detailed investigations of the resonance region neutron-capture cross sections [44]. With the higher production rates at FRIB and access to new tools to study neutron capture reactions, additional cross-section measurements relevant to stockpile stewardship and nuclear astrophysics could be pursued.

ACKNOWLEDGMENTS

We acknowledge the staff of the NSCL, particularly the operation and A1900 staff for experiment coordination and providing beam. We thank J. Yurkon for Au-sputtering of the Ti window. We thank P. T. Wooddy for nuclear counting support and R. Lindvall for the ICPMS analysis. We also thank the operators and radiation safety staff at MURR and MNRC for experimental support at the reactors. At LLNL,

this work was funded through LDRD 16-ERD-022 and was performed under the auspices of the US Department of Energy under Contract No. DE-AC52-07NA27344. S.R.M. and G.F.P. were supported under DESC0013662. S.E.L. and C.S.L. were supported by the US Department of Energy under Grant No. DESC0015558.

[1] E. P. Abel, M. Avilov, V. Ayres, E. Birnbaum, G. Bollen, G. Bonito, T. Bredeweg, H. Clause, A. Couture, J. Devore, M. Dietrich, P. Ellison, J. Engle, R. Ferrieri, J. Fitzsimmons, M. Friedman, D. Georgobiani, S. Graves, J. Greene, S. Lapi *et al.*, Isotope harvesting at FRIB: additional opportunities for scientific discovery, J. Phys. G: Nucl. Part. Phys. **46**, 100501 (2019).

[2] D. Schumann, J. Neuhausen, I. Dillmann, C. Domingo Pardo, F. Käppeler, J. Marganiec, F. Voss, S. Walter, M. Heil, R. Reifarth, J. Goerres, E. Uberseder, M. Wiescher, and M. Pignatari, Preparation of a ^{60}Fe target for nuclear astrophysics experiments, Nucl. Instrum. Methods Phys. Res., Sect. A **613**, 347 (2010).

[3] G. Rugel, T. Faestermann, K. Knie, G. Korschinek, M. Poutivtsev, D. Schumann, N. Kivel, I. Günther-Leopold, R. Weinreich, and M. Wohlmuther, New Measurement of the ^{60}Fe Half-Life, Phys. Rev. Lett. **103**, 072502 (2009).

[4] A. Wallner, M. Bichler, K. Buczak, R. Dressler, L. K. Fifield, D. Schumann, J. H. Sterba, S. G. Tims, G. Wallner, and W. Kutschera, Settling the Half-Life of ^{60}Fe: Fundamental for a Versatile Astrophysical Chronometer, Phys. Rev. Lett. **114**, 041101 (2015).

[5] K. M. Ostdiek, T. S. Anderson, W. K. Bauder, M. R. Bowers, A. M. Clark, P. Collon, W. Lu, A. D. Nelson, D. Robertson, M. Skulski, R. Dressler, D. Schumann, J. P. Greene, W. Kutschera, and M. Paul, Activity measurement of ^{60}Fe 60 through the decay of ^{60m}Co and confirmation of its half-life, Phys. Rev. C **95**, 055809 (2017).

[6] E. Uberseder, R. Reifarth, D. Schumann, I. Dillmann, C. D. Pardo, J. Gorres, M. Heil, F. Kappeler, J. Marganiec, J. Neuhausen, M. Pignatari, F. Voss, S. Walter, and M. Wiescher, Measurement of the ^{60}Fe$(n,g)^{61}$Fe Cross Section at Stellar Temperatures, Phys. Rev. Lett. **102**, 151101 (2009).

[7] T. Heftrich, M. Bichler, R. Dressler, K. Eberhardt, A. Endres, J. Glorius, K. Göbel, G. Hampel, M. Heftrich, F. Käppeler, C. Lederer, M. Mikorski, R. Plag, R. Reifarth, C. Stieghorst, S. Schmidt, D. Schumann, Z. Slavkovská, K. Sonnabend, A. Wallner, M. Weigand, N. Wiehl, and S. Zauner, Thermal neutron capture cross section of the radioactive isotope ^{60}Fe, Phys. Rev. C **92**, 015806 (2015).

[8] D. Schumann, N. Kivel, and R. Dressler, Production and characterization of ^{60}Fe standards for accelerator mass spectrometry, PLoS One **14**, 6 (2019).

[9] M. Ayranov and D. Schumann, Preparation of ^{26}Al, ^{59}Ni, ^{44}Ti, ^{53}Mn, and ^{60}Fe from a proton irradiated copper beam dump, J. Radiol. Nucl. Chem. **286**, 649 (2010).

[10] S. Heinitz, D. Kiselev, N. Kivel, and D. Schumann, Separation of weighable amounts of ^{10}Be from proton irradiated graphite, Appl. Radiat. Isot. **130**, 260 (2017).

[11] B. D. Schumann, T. Stowasser, R. Dressler, and M. Ayranov, Possibilities of preparation of exotic radionuclide samples at PSI for scientific investigations, Radiochim. Acta **101**, 501 (2013).

[12] A. Pen, T. Mastren, G. F. Peaslee, K. Petrasky, P. A. Deyoung, D. J. Morrissey, and S. E. Lapi, Design and construction of a water target system for harvesting radioisotopes at the National Superconducting Cyclotron Laboratory, Nucl. Instrum. Methods Phys. Res., Sect. A **747**, 62 (2014).

[13] T. Mastren, A. Pen, G. F. Peaslee, N. Wozniak, S. Loveless, S. Essenmacher, L. G. Sobotka, D. J. Morrissey, and S. E. Lapi, Feasibility of isotope harvesting at a projectile fragmentation facility: ^{67}Cu, Sci. Rep. **4**, 1 (2014).

[14] T. Mastren, A. Pen, S. Loveless, B. V. Marquez, E. Bollinger, B. Marois, N. Hubley, K. Brown, D. J. Morrissey, G. F. Peaslee, and S. E. Lapi, Harvesting ^{67}Cu from the collection of a secondary beam cocktail at the National Superconducting Cyclotron Laboratory, Anal. Chem. **87**, 10323 (2015).

[15] C. S. Loveless, B. E. Marois, S. J. Ferran, J. T. Wilkinson, L. Sutherlin, G. Severin, J. A. Shusterman, N. D. Scielzo, M. A. Stoyer, D. J. Morrissey, J. D. Robertson, G. F. Peaslee, and S. E. Lapi, Harvesting ^{48}V at the National Superconducting Cyclotron Laboratory, Appl. Radiat. Isot. **157**, 1 (2020).

[16] E. P. Abel, H. K. Clause, and G. W. Severin, Radiolysis and radionuclide production in a flowing-water target during fast ^{40}Ca^{20+} irradiation, Appl. Radiat. Isot. **158**, 1 (2020).

[17] T. Kobayashi, T. Sasaki, I. Takagi, and H. Moriyama, Solubility of zirconium(IV) hydrous oxides, J. Nucl. Sci. Technol. **44**, 90 (2007).

[18] M. A. Deri, B. M. Zeglis, L. C. Francesconi, and J. S. Lewis, PET imaging with ^{89}Zr: From radiochemistry to the clinic, Nucl. Med. Biol. **40**, 3 (2013).

[19] A. Baimukhanova, V. Radchenko, J. Kozempel, A. Marinova, V. Brown, V. Karandashev, D. Karaivanov, P. Schaffer, and D. Filosofov, Utilization of (p,4n) reaction for ^{86}Zr production with medium energy protons and development of a ^{86}Zr $\rightarrow$ ^{86}Y radionuclide generator, J. Radiol. Nucl. Chem. **316**, 191 (2018).

[20] K. Sonnabend, P. Mohr, A. Zilges, R. Hertenberger, H.-F. Wirth, G. Graw, and T. Faestermann, First excited state of the *s*-process branching nucleus ^{95}Zr, Phys. Rev. C **68**, 048802 (2003).

[21] R. D. Hoffman, K. Kelley, F. S. Dietrich, R. Bauer, and M. Mustafa, Lawrence Livermore National Laboratory Technical Report No. UCRL-TR-222275 (Lawrence Livermore National Laboratory, 2006).

[22] A. C. Larsen, M. Guttormsen, R. Schwengner, D. L. Bleuel, S. Goriely, S. Harissopulos, F. L. Bello Garrote, Y. Byun, T. K. Eriksen, F. Giacoppo, A. Görgen, T. W. Hagen, M. Klintefjord, T. Renstrøm, S. J. Rose, E. Sahin, S. Siem, T. G. Tornyi, G. M. Tveten, A. V. Voinov, and M. Wiedeking, Experimentally constrained $(p,\gamma)^{89}$Y and $(n,\gamma)^{89}$Y reaction rates relevant to *p*-process nucleosynthesis, Phys. Rev. C **93**, 045810 (2016).

[23] V. Reis, R. Hanrahan, and K. Levedahl, The Big Science of stockpile stewardship, Phys. Today **69**(8), 46 (2016).

[24] R. J. Prestwood, K. W. Thomas, D. R. Nethaway, and N. L. Smith, Measurement of 14-MeV neutron cross sections for ^{88}Zr and ^{88}Y, Phys. Rev. C **29**, 805 (1984).

[25] J. A. Shusterman, N. D. Scielzo, K. J. Thomas, E. B. Norman, S. E. Lapi, C. S. Loveless, N. J. Peters, J. D. Robertson, D. A. Shaughnessy, and A. P. Tonchev, The surprisingly large neutron capture cross-section of ^{88}Zr, Nature (London) **565**, 328 (2019).

[26] P. L. Brown, E. Curti, B. Grambow, and C. Ekberg, in *Chemical Thermodynamics of Zirconium, Vol. 8*, edited by F. J. Mompean, J. Perrone, and M. Illemassene (OECD Nuclear Energy Agency, Paris, 2005).

[27] A. Stolz, T. Baumann, T. Ginter, D. Morrissey, M. Portillo, B. Sherrill, M. Steiner, and J. Stetson, Production of rare isotope beams with the NSCL fragment separator, Nucl. Instrum. Methods Phys. Res. B **241**, 858 (2005).

[28] D. J. Morrissey, B. M. Sherrill, M. Steiner, A. Stolz, and I. Wiedenhoever, Commissioning the A1900 projectile fragment separator, Nucl. Instrum. Methods Phys. Res. B **204**, 90 (2003).

[29] E. A. McCutchan and A. A. Sonzogni, Nuclear data sheets for A = 88, Nucl. Data Sheets **115**, 135 (2014).

[30] C. Ekberg, G. Källvenius, Y. Albinsson, and P. L. Brown, Studies on the hydrolytic behavior of zirconium(IV), J. Solution Chem. **33**, 47 (2004).

[31] B. Singh, Nuclear data sheets for A = 89, Nucl. Data Sheets **114**, 1 (2013).

[32] H. Yücel and M. Karadag, Experimental determination of the α-shape factor in the $1/E^{1+\alpha}$ epithermal-isotopic neutron source-spectrum by dual monitor method, Ann. Nucl. Energy **31**, 681 (2004).

[33] A. Koning, D. Rochman, J. C. Sublet, N. Dzysiuk, M. Fleming, and S. van der Marck, TENDL: Complete nuclear data library for innovative nuclear science and technology, Nucl. Data Sheets **155**, 1 (2019).

[34] H. Harada, S. Nakamura, T. Katoh, and Y. Ogata, Measurement of thermal neutron cross section and resonance integral of the reaction ^{99}Tc$(n,\gamma)^{100}$Tc, J. Nucl. Sci. Technol. **32**, 395 (1995).

[35] S. Nakamura, K. Furutaka, H. Wada, T. Fujii, H. Yamana, T. Katoh, and H. Harada, Measurement of thermal neutron capture cross section and resonance integral of the ^{90}Sr$(n,\gamma)^{91}$Sr Reaction, J. Nucl. Sci. Technol. **38**, 1029 (2001).

[36] C. L. Duncan and K. S. Krane, Neutron capture cross section of ^{102}Pd, Phys. Rev. C **71**, 054322 (2005).

[37] S. Mughabghab, Thermal neutron capture cross sections, resonance integrals and G-factors, Technical Report No. INDC(NDS)-440 (International Atomic Energy Agency, Vienna, 2003).

[38] A. Y. Dauenhauer and K. S. Krane, Neutron capture cross sections of ^{130,132,134,136,138}Ba, Phys. Rev. C **85**, 064301 (2012).

[39] B. Pritychenko and S. F. Mughabghab, Neutron thermal cross sections, Westcott factors, resonance integrals, Maxwellian averaged cross sections and astrophysical reaction rates calculated from the ENDF/B-VII.1, JEFF-3.1.2, JENDL-4.0, ROSFOND-2010, CENDL-3.1 and EAF-2010 evaluated data libraries, Nucl. Data Sheets **113**, 3120 (2012).

[40] K. A. Domnanich, E. P. Abel, H. K. Clause, C. Kalman, W. Walker, and G. W. Severin, An isotope harvesting beam blocker for the National Superconducting Cyclotron Laboratory, Nucl. Instrum. Methods Phys. Res., Sect. A **959**, 163526 (2020).

[41] M. D. Scott, J. Schorp, L. Sutherlin, and J. D. Robertson, Isotope harvesting with hollow fiber supported liquid membrane (HFSLM), Appl. Radiat. Isot. **157**, 109027 (2020).

[42] M. K. Pandey, H. P. Engelbrecht, J. P. Byrne, A. B. Packard, and T. R. DeGrado, Production of ^{89}Zr via the ^{89}Y$(p,n)^{89}$Zr reaction in aqueous solution: Effect of solution composition on in-target chemistry, Nucl. Med. Biol. **41**, 309 (2014).

[43] N. A. Zacchia, D. M. Martinez, and C. Hoehr, Radiolysis reduction in liquid solution targets for the production of ^{89}Zr, Appl. Radiat. Isot. **155**, 1 (2020).

[44] P. E. Koehler, J. L. Ullmann, A. J. Couture, and S. M. Mosby, Attempting to close the loop on the Oslo technique at ^{198}Au: Constraining the nuclear spin distribution, in *Compound-Nuclear Reactions: Proceedings of the 6th International Workshop on Compound-Nuclear Reactions and Related Topics CNR*18, Berkeley, CA, 2018* (Springer, Berlin, 2021), pp. 187–193.